DTIC FILE COPY

(2)

PENNSTATE

ARL

DTIC
ELECTE
FEB 21 1990
S D
CO D

AD-A218 318

Annual Report
1 February 1989 to 31 January 1990

SEA-WATER MAGNETOHYDRODYNAMIC PROPULSION FOR NEXT-GENERATION UNDERSEA VEHICLES

Sponsored By

Department of the Navy
Office of Naval Research
Grant No. N00014-89-J-1693

DISTRIBUTION STATEMENT A
Approved for public release
Distribution Unlimited

Prepared By

T. F. Lin, J. B. Gilbert, R. Kossowsky
February 1990

Applied Research Laboratory and
The Nuclear Engineering Department
The Pennsylvania State University
P.O. Box 30
State College, PA 16804

90 02 13 098

PENNSTATE

ARL

Annual Report
1 February 1989 to 31 January 1990

SEA-WATER MAGNETOHYDRODYNAMIC PROPULSION FOR NEXT-GENERATION UNDERSEA VEHICLES

Sponsored By

Department of the Navy
Office of Naval Research
Grant No. N00014-89-J-1693

Prepared By

T. F. Lin, J. B. Gilbert, R. Kossowsky

February 1990

Applied Research Laboratory and
The Nuclear Engineering Department
The Pennsylvania State University
P.O. Box 30
State College, PA 16804

ABSTRACT

Three tasks were performed in this report period. Their individual abstracts are summarized as follows:

(I) Thruster Performance Modelings - The purpose of this work is to analyze underwater vehicle propulsion by applying Lorentz forces to the surrounding sea water. While this propulsion concept involves two different schemes, i.e. the external field method and the internal duct-type method, the current analysis focuses on the internal thruster scheme due to the space limitations and speed considerations. The theories of magnetohydrodynamic (MHD) pump jet propulsion are discussed. A so-called "dual control volume" analysis to model the MHD thruster, and calculations of vehicle velocity and power efficiency are presented. Optimization of mechanical thrust are conclusively discussed. Different classes of underwater vehicles are considered. They include smaller vehicles such as torpedoes, remotely operated vehicles (ROV), underwater autonomous vehicles (UAV), up to larger ones such as submarines. The analytical results indicated that the speed performance increases proportionally with the sea-water conductivity, and with the square of the magnetic field strength. At the same time, the energy efficiencies of vehicles appeared to favor larger systems with longer MHD channel.

(II) Sea Water Conductivity Enhancement –

This work discusses the mechanisms of enhancing the electric conductivity of sea water. The direct impact of conductivity enhancement of sea water is the improvement of propulsion performances of marine vehicles that use the magnetohydrodynamic thrusts of sea water. The performance improvement can be in energy efficiency or in vehicle speed. Injection of strong electrolytes (acids or bases) into the main sea water flow in the MHD channel appeared to be the most logical way of achieving the purpose. Several seeding compounds were compared from the electrochemical points of view. The advantage of using concentrated sulfuric acid (H_2SO_4) over the others was conclusively discussed. It was found that the computed conductivity of a synthetic sea water of known salt constituency is consistent with the average conductivity of ocean water. Parametric studies of volumetric mixing ratios and seeding electrolytes were also

conducted, and their effects on the conductivity of the mixed sea water were compared and discussed.

(III) Status of Current Superconductivity Works

A survey of recent research in both low-T_c and high-T_c superconductivities is provided. It is still generally true that high-T_c superconductors carry critical current densities several orders of magnitude less than those of low-T_c ones. However, although in early stages, development of bismuth-based high-T_c superconductors is showing comparable critical current densities with those of niobium-based superconductors.

STATEMENT "A" per Dr. G. Roy
NRL/Code 1132P
TELECON 2/21/90 CG

per call

DTIC COPY INSPECTED 8

A-1

TABLE OF CONTENTS

Page

ABSTRACT ii

TABLE OF CONTENTS iv

LIST OF TABLES v

LIST OF FIGURES vi

NOMENCLATURE vii

ACKNOWLEDGEMENT x

I. THRUSTER PERFORMANCE MODELINGS 1

I.1 Introduction 1

I.2 Theoretical Analyses 2

I.2.1 Analysis of the MHD pump 2

I.2.2 Dual-control-volume analysis 4

I.2.3 Solution procedure 6

I.3 Results 7

I.4 Discussion 9

II. SEA WATER CONDUCTIVITY ENHANCEMENT 22

II.1 Introduction 22

II.2 Analyses 23

II.3 Results 27

II.4 Discussion 28

III. STATUS OF CURRENT SUPERCONDUCTIVITY WORKS 32

REFERENCES 37

LIST OF TABLES

Table	Page
1. Properties of common seeding electrolytes at 20°C	29
2. Conductivity contributions of different electrolytes	30

LIST OF FIGURES

Figure		Page
1(a)	Submersible with an annular MHD channel	12
1(b)	Submersible with rectangular MHD channels	12
2.	Schematic of a duct-type MHD channel	13
3.	Control volume # 1	14
4.	Control volume # 2	14
5.	Velocity vs. magnetic field for class 1 vehicles	15
6.	Velocity of class 1 vehicles at B=20T	16
7.	Total efficiency of class 1 vehicles at B=20T	17
8.	Thrust of class 1 vehicles at B=20T	18
9.	Velocity of class 2 vehicles at B=5T	19
10.	Total efficiency of class 2 vehicles at B=5T	20
11.	Thrust of class 2 vehicles at B=5T	21
12.	Conductances of sea water seeded with electrolytes	31
13.	Critical current density of Bi-2212/Ag and $YBa_2Cu_3O_7$/Ag-wire at 4.2K in comparison with commercial NbTi, Nb_3Sn, and $(Nb,Ta)_3$ multifilamentary wires (non-copper J_c) as produced by Vacuumschmelze	36

NOMENCLATURE

Part I:

A_{ex}	exit area of the MHD channel (m^2).
A_{in}	entrance area of the MHD channel (m^2).
A_{surf}	surface area of the vehicle.
B	magnetic field strength (Teslas).
C	nozzle discharge coefficient.
C_D	drag coefficient of vehicle surface.
D	electrode gap distance (m).
D_H	equivalent hydraulic diameter (m).
E	flow-induced counter electric field (volt/m).
F	velocity-of-approach factor of a nozzle.
F_{em}	Lorentz force (Newtons).
f	Darcy-Weisbach friction factor for pipe flows.
I	current across the electrodes (Amp).
L	active length of the MHD channel (m).
$\dot{m}$	mass flowrate in an MHD channel (kg/s).
N_{ch}	number of MHD channels.
P_e	electrical power required by the MHD channel (watts).
P_w	mechanical power imparted to the sea water in the MHD channel (watts).
p_{amb}	ambient pressure of the vehicle (Pa).
p_{in}	entrance pressure of an MHD channel (Pa).
p_{ex}	exit pressure of an MHD channel (Pa).
R	resistance of sea water in the MHD channel (Ohms).
s	area ratio between the nozzle exit and the channel entrance (A_{ex}/A_{in}).
T	thrust of an MHD channel (Newtons).
U_{ex}	velocity of the sea water exiting from the nozzle (m/s).

U_{in} velocity of the sea water in the channel (m/s).

V voltage across the electrodes (volts).

V_s velocity of the vehicle (m/s or knots).

V_{ch} active volume of sea water in the MHD channel (m^3).

W width of the electrode (m).

Y nozzle expansion coefficient.

Δp_{ch} pressure rise or drop across the entire MHD channel (Pa).

Δp_N pressure drop across nozzle (Pa).

η_e electric efficiency.

η_{ind} field induction efficiency.

η_t total efficiency.

σ electric conductivity of sea water ($1/(\Omega \cdot m)$).

ρ sea water density (kg/m^3).

Part II:

A electrode area (m^2).

c mole concentration (mol/l).

c_o mole concentration of electrolyte solution before injection (mol/l).

L conductance (Ω^{-1}).

l length of the conductivity cell (m).

R resistance (Ω).

r volumetric mixing ratio of electrolyte solution to the mixed sea water.

ρ specific resistance (Ωm).

σ specific conductance ($\Omega^{-1}m^{-1}$).

σ_{sw} specific conductance of sea water ($\Omega^{-1}m^{-1}$).

σ_a specific conductance contribution from the injected electrolyte ($\Omega^{-1}m^{-1}$).

ν_+ number of positive ions by the electrolyte formula.

ν_- number of negative ions by the electrolyte formula.

λ°_{+} molar ionic conductance of positive ions ($\Omega^{-1}m^2mol^{-1}$).

λ°_{-} molar ionic conductance of negative ions ($\Omega^{-1}m^2mol^{-1}$).

Λ molar conductance ($\Omega^{-1}m^2mol^{-1}$).

Λ° limiting molar conductance ($\Omega^{-1}m^2mol^{-1}$).

ACKNOWLEDGEMENT

This work was supported mainly by Office of Naval Research Grant No: N00014-89-J-1693 with Dr. Gabriel D. Roy as Scientific Officer, and in part by Applied Research Laboratory of the Pennsylvania State University.

PART I
THRUSTER PERFORMANCE MODELINGS

I.1 Introduction

Sea water conducts electricity in a modest scale by electrolytic ion exchange. While its conductivity is several orders of magnitude lower than metals, it is significantly higher than fresh water. By taking advantage of sea water's modest electric characteristics, the electromagnetic propulsion of marine vehicles has been a subject of technical speculation and study for some years.[1-6] The concept did not appear to hold much promise until the advent of the superconducting magnet. With such a magnet, the power requirement for excitation is virtually absent, and the weight penalty of the magnet is drastically reduced. Also, much stronger magnetic field than those previously attainable can be realized. Nevertheless, the only proof of its technical possibility was carried out more than twenty years ago by S. Way et al.[6] In that, a vehicle 4-ft long and 18-inch in diameter was propelled by such an MHD propulsion principle at a speed only about 1 ft/s. The magnet used was a heavy electro-magnet, and S. Way had concluded that superconducting magnets are essential for the technology to be practical.

International activities in this subject were also visible. The U.S.S.R. have conceived its application in large icebreaker propulsion.[7] More recently, Japan has developed a strong program in researching the electro-magnetic thrusters (EMT) for her future freighters.[8-10] With the recent advances in high-T_c superconductors and the possible simplification in cryogenics, it now appears that there is even more technical possibility in realizing a sea-water MHD propelled underwater vehicle. Whether such a vessel will be economically attractive or not is a question that must await further investigation. However, it is fair to predict that in certain naval applications where the importance of acoustic signature of a vehicle is outweighing other considerations, the MHD technology offers superior quietness because of its reduced mechanical moving parts.

In the consideration of duct-type internal MHD thrusters, the electric current and magnetic

field in the sea water are normally arranged to be orthogonal to each other in the channel to provide an optimal Lorentz (j x B) force. Sea water is being pumped in a straight active section of the channel. Immediately following that the sea water is pushed through a smooth nozzle that provides an adequate momentum thrust to makes the vehicle move. However, a thruster without a smooth converging nozzle is also possible in which the main thrust comes from the pressure increase in the channel. The following section discusses the detail theoretical development of this type of MHD pump jet propulsion. The vehicle performances in speed and efficiency are also discussed.

I.2 Theoretical Analyses

The general configurations of submerged vehicles with duct-type MHD thrusters can be shown in Figures 1(a) and 1(b). The basic pump jet propulsion principles are essentially the same in these two schemes. In both cases, the electric current and the magnetic field are arranged to be perpendicular to each other in an active region of the MHD channel. Sea water is brought in from the front end of a channel. As the Lorentz forces are applied to the channel, they pump the sea water downstream and eject it from the nozzle with a higher speed. The difference in speed between inlet and outlet of the channel creates the momentum thrust that pushes the vehicle forward. Again, if no converging nozzle is present, the pressure build-up in the channel would be the main mechanism for propulsion. It is worth noticing that rotating machinery such as propeller is not required in such a system. In general, the annular channel thruster (Fig. 1(a)) provides a better efficiency because the amount of friction surface area per unit volume of fluid in the channel is minimized. However, the scheme with separate rectangular channels provides the ability to steer and maneuver the vehicle by individually controlling the thrust of the channel.

I.2.1 Analysis of the MHD pump

A schematic of an MHD channel is shown in Figure 2, in that a simple rectangular thruster is illustrated. An analysis of annular thruster like the one shown in Fig. 1(a) will be very

similar. The electric current is supplied by the electrodes from the top to the bottom, and the magnetic field is pointed into the paper so as to be perpendicular to the current. The Lorentz force is directed to the right to push the sea water through the nozzle. The net current flowing across the MHD channel between the electrodes is,

$$I = \frac{V - ED}{R}, \tag{1}$$

where D is the electrode gap distance, E is the flow-induced electric field whose direction is anti-parallel to I, and R is the electric resistance of sea water in the channel. If the width and length of the electrodes are W and L respectively, then the resistance is,

$$R = \frac{D}{\sigma W L}, \tag{2}$$

where σ is the electric conductivity of sea water ranging from 4 to 5 $1/(\Omega m)$. The first order magnetohydrodynamic approximations are then taken to assume only the induced electric field is significant, but not the induced magnetic field. Thus,

$$E = BU_{in}, \tag{3}$$

where U_{in} is the velocity of sea water in the channel. Defining the field induction efficiency to be,

$$\eta_{ind} = \frac{ED}{V} = \frac{BU_{in}D}{V}, \tag{4}$$

and the net current becomes,

$$I = \frac{1 - \eta_{ind}}{\eta_{ind}} \sigma B U_{in} W L. \tag{5}$$

The total Lorentz force pushing the sea water in the channel is,

$$F_{em} = IDB = \frac{1 - \eta_{ind}}{\eta_{ind}} \sigma B^2 U_{in} DWL = \frac{1 - \eta_{ind}}{\eta_{ind}} \sigma B^2 U_{in} V_{ch}, \tag{6}$$

where V_{ch} is the active volume of the channel.

The mechanical power imparted on the sea water in the channel is,

$$P_w = F_{em} U_{in} = \frac{1 - \eta_{ind}}{\eta_{ind}} \sigma B^2 U_{in}^2 V_{ch}. \tag{7}$$

The electrical power supplied to the MHD channel is,

$$P_e = VI = \frac{1-\eta_{ind}}{\eta_{ind}} \sigma B V U_{in} W L, \tag{8}$$

and the electrical efficiency is defined as, from Eqs. (7) and (8),

$$\eta_e = \frac{P_w}{P_e} = \frac{BU_{in}D}{V}. \tag{9}$$

This is identical to the field induction efficiency, η_{ind}. This, however, does not mean one can extract the most mechanical power from the MHD channel at η_e (or η_{ind}) being equal to 1. As one can see from Eq. (8), P_e approaches to zero as η_e approaches to unity. From Eqs. (7) and (9), the expression for the mechanical power under fixed channel dimensions and electrical potential would be,

$$P_w = (1-\eta_e)\eta_e \sigma V^2 \frac{V_{ch}}{D^2}. \tag{10}$$

P_w can be optimized by taking the derivative of Eq. (10) with respect to η_e, and determining the value of η_e that satisfies a zero derivative. It turns out that P_w is optimized when η_e is equal to 0.5. That also means 50% of the electrical power will be consumed as heat by Ohmic loss. This is a condition that will always have to be taken into account in the thruster design.

I.2.2 Dual-control-volume analysis

In the past, the analyses of sea water MHD thrusters have been based on Bernoulli's equations in modeling momentum exchanges.[7,11] These analytical approaches basically ignored the viscous dissipation of fluid in the channel, and the pressures at the entrance and exit (p_{in} and p_{ex}) were taken to be the same as the ambient pressure. These, in reality, were not quite justified. In our current analytical models, two separate control volumes are considered, to take into accounts the viscous dissipation in the channel and the relationship between the thrusts and the performances of the vehicle. In doing so, the pressure conditions at the inlet and outlet of each channel must be computed, instead of being assumed. Similarly to rocket propulsion, this would make up the pressure thrust portion of the total thrust.

The first control volume, shown as dotted lines in Figure 3, is the sea water volume enclosed by an individual MHD channel. The mass and momentum balances of flow around this control

volume are discussed as follows. Assuming the ratio between the nozzle exit area and the MHD channel area is s, the mass conservation yields,

$$U_{ex} = \frac{U_{in}}{s}, \tag{11}$$

and the momentum conservation yields,

$$\rho U_{in} A_{in}(U_{ex} - U_{in}) = IBD - (f\frac{L}{D_H}\frac{\rho U_{in}^2}{2})A_{in} - \Delta p_N A_{in} + (p_{in}A_{in} - p_{ex}A_{ex}). \tag{12}$$

The second term in the right hand side (RHS) of Eq. (12) accounts for the friction loss in the straight channel, and the third term accounts for the nozzle loss. Also in Eq. (12), D_H is the equivalent hydraulic diameter of the channel, and f is the Darcy-Weisbach friction factor that is a function of the Reynold's number of the pipe flow. Although equivalent diameters are used in Eq. (12) for non-circular channels, f has been found to be slightly over-predicting the friction.[12] The nozzle loss is proportional to the square of the mass flowrate through it. It can be expressed as,[13]

$$\Delta p_N = \frac{1}{2\rho}\frac{\dot{m}^2}{(YFCA_{ex})^2}, \tag{13}$$

where Y is the expansion factor which is unity for liquids. F is the velocity-of-approach factor defined as $F = 1/\sqrt{1-s^2}$. C is the nozzle discharge coefficient which has a value approximately equal to 0.98 for smooth nozzle transition at high Reynold's number. The last term in the RHS of Eq. (12) is the net pressure force from both the inlet and outlet of a channel.

The thrust that is put out by an MHD channel can be written as, from the momentum principles,[14]

$$T = \dot{m}(U_{ex} - U_{in}) + (p_{ex}A_{ex} - p_{in}A_{in}) + p_{amb}(A_{in} - A_{ex}). \tag{14}$$

The first term in the RHS of Eq. (14) is the momentum thrust, and the combination of the second and third terms is the pressure thrust. p_{amb} is the ambient pressure of the vehicle, and is a depth-dependent quantity. From Eq. (12), Eq. (14) can be re-written as,

$$T = \Delta p_{ch}A_{in} + p_{amb}(A_{in} - A_{ex}), \tag{15}$$

where Δp_{ch} is the pressure rise (or drop) across the entrance and exit of the MHD channel. It is defined as,

$$\Delta p_{ch} A_{in} = (p_{ex} - p_{in}) A_{in} = IBD - (f \frac{L}{D_H} \frac{\rho U_{in}^2}{2}) A_{in} - \Delta p_N A_{in}. \tag{16}$$

The relationship between the total thrust of all the MHD channels and the vehicle velocity can be obtained from the second control volume, shown as dotted lines in Figure 4. The skin friction of a vehicle is proportional to the square of its velocity, and must be balanced by the total thrust provided by the MHD thrusters at steady state. The equation describing the force balance in the second control volume is,

$$C_D A_{surf} (\frac{1}{2} \rho V_s^2) = N_{ch} T, \tag{17}$$

where N_{ch} is the total numbers of MHD channels, A_{surf} is the total vehicle surface area. C_D is the drag coefficient at the vehicle surface, which is obtained from the standard values of International Towing Tank Conference[15,16] (ITTC, 1957). The thrust in Eq. (14) can also be reduced to,

$$T = \dot{m}(U_{ex} - U_{in}) - (p_{in} - p_{amb})(A_{in} - A_{ex}) + \Delta p_{ch} A_{ex}, \tag{18}$$

and the term $(p_{in} - p_{ex})$ can be approximated as an entrance pressure defect, from the Bernoulli's equation,

$$p_{in} - p_{amb} = \frac{1}{2} \rho (V_s^2 - U_{in}^2). \tag{19}$$

From Eqs. (18) and (19), Eq. (17) becomes,

$$C_D A_{surf} (\frac{1}{2} \rho V_s^2) = N_{ch} (\dot{m}(U_{ex} - U_{in}) - \frac{1}{2} \rho (V_s^2 - U_{in}^2)(A_{in} - A_{ex}) + \Delta p_{ch} A_{ex}). \tag{20}$$

I.2.3 Solution procedures

In the discussion of the "dual control volume" analysis above, the pressures at the entrance and exit of an MHD channel were treated as unknowns. The relation between them was formulated in Eq. (16). If the vehicle dimensions and the MHD channel dimensions are given, the applied voltage that gives the optimal electric efficiency can be determined for given B and

U_{in} from Eq. (4) by letting $\eta_{ind} = 0.5$. Then, Δp_{ch} can be calculated from Eq. (16) for a given s (nozzle area ratio). Eq. (20) in turn becomes a quadratic equation of V_s, which can be readily solved. However, there exists only a unique s which is less than 1 for a given U_{in} to satisfy the condition in Eq. (15). It is also noted that Eq. (15) involves the ambient pressure of the vehicle. For a given depth, iterative procedures such as the generalized Newton's method or the bi-sectional method can be applied for the solution of s.

Here it is convenient to define the three terms in the RHS of Eq. (20) as the momentum thrust, pressure thrust 1 and pressure thrust 2, respectively. It is noted that, when $s = 1$ (no converging nozzle), both the momentum thrust and pressure thrust 1 are zero, yielding Eq. (20) identically the same as Eq. (15). That means $s = 1$ in the present study is always a solution. However, the solutions ($s < 1$ or $s = 1$) may or may not be physically valid. It depends on whether the resulting vehicle velocity would give a thrusting power that violates the imposed 50% electric efficiency or not.

As a result, the performances of a vehicle with MHD thrusters can be analyzed by plotting the vehicle velocity, the total efficiency and the different thrust components against the sea water velocity in the channel. Here, the total efficiency is defined as,

$$\eta_t = \frac{N_{ch} T V_s}{P_e}. \tag{21}$$

For each point in a performance curve, there is a corresponding s to satisfy the conditions imposed by the conservation laws in both control volumes. This s value directly influence the nozzle design.

I.3 Results

Performance calculations were based on two classes of underwater vehicles. The first class (class 1) is vehicles with dimensions similar to MK48 torpedoes. The common diameter and length were chosen to be 0.533 meter and 6.1 meters, respectively. The second class (class 2) is large submersibles such as submarines, with vessel diameter and length being 9.8 meters

and 83 meters, respectively. Four rectangular MHD channels were attached to each vehicle 90 degrees apart from one another (Fig. 1(b)), and the channel lengths were always chosen to be two thirds of the vehicle lengths. For the first class vehicles, the electrode width and gap distance were 0.3 meter and 0.1 meter. For the second class vehicles, the electrode width and gap distance were 3 meters and 1 meter, respectively.

Figure 5 shows the dependence of class 1 vehicle velocity on the magnetic field strength and the sea water conductivity. It indicates that the vehicle velocity increases proportionally with σB^2. The solid line represents the velocity performance at realistic sea water conditions. To achieve the torpedo speed (50 - 70 knots), the magnetic field needs to be as large as 15 to 20 Teslas, which are very large fields. Nevertheless, it points to the possibility of low speed applications of ROV or UAV with more realistic magnetic fields, i.e. less than 10 Teslas. By increasing the conductivity of sea water in the active volume of the MHD channels, shown as dashed line, the velocity can be increased linearly. Similar curves can also be generated for class 2 vehicles. For a reasonable submarine velocity, a magnetic field of about 5 Teslas would be sufficient. This will be further discussed next.

Figures 6, 7 and 8 show the velocity, efficiency and thrust performances of class 1 vehicles, vs. the fluid velocity in the MHD channel at B = 20 Teslas. In general, the vehicle velocity increases with channel flow, as a result of increasing MHD pumping. As discussed in the theoretical analyses section, there can exist two satisfactory solutions for V_s at low U_{in} due to the quadratic nature of Eq. (20). One solution corresponds to the case of s = 1, where the MHD channel is straight and without any nozzle. This solution, shown as the upper curves in Figs. 6 and 7, is not valid when η_t becomes larger than 0.5. This contradicts the imposed condition of optimal electric efficiency, as discussed in the analyses of MHD pump. The other solution corresponds to a s value less than 1. It suggests that the existence of a smooth nozzle would create a higher U_{ex} which in turn would generate a momentum thrust. This is often a valid solution and is shown as the lower curves in the figures. Valid solution normally exists for s = 1 at higher velocity. In this situation, the vehicle thrust is only from the pressure thrust.

Although the total efficiency generally decrease with increasing U_{in}, for class 1 vehicles, there appears to have an optimal efficiency near $\eta_t = 0.40$, Fig. 7. In Fig. 8, the total thrust and its various thrust components of a single thrust channel are plotted. To the RHS of the plot where s is equal to 1, since the momentum thrust and pressure thrust 1 are both zero, the total thrust is simply equal to the pressure thrust 2. It is noted that the momentum thrust is always greater or equal to zero, pressure thrust 1 is always smaller or equal to zero, and pressure thrust 2 can be greater or smaller to zero. The total thrust increases with increasing channel flow as physically expected. However, its increase is more rapid at low channel flow which corresponds to high momentum thrust at low nozzle area ratio.

Figures 9, 10 and 11 show the velocity, efficiency and thrust performances of class 2 vehicles, i.e. submarines. It is noted that reasonable submarine velocity can be achieved with a magnetic field of about 5 Teslas. For a submarine having a 35 knots velocity, the total power efficiencies are about 0.35 and 0.45 for $s < 1$ and $s = 1$, respectively. This is largely due to the large size of the MHD channels. The thrust components of class 2 vehicles are very similar to those of class 1 vehicles. For class 2 vehicles, even larger MHD channels than the ones currently under consideration are possible. That would result in further increases in vehicle velocity and total efficiency. Results in Figs. 6-11 are based on the condition that vehicles are at a depth 30 meters below the surface.

I.4 Discussion

The purpose of this study is to assess the feasibility of sea water MHD propulsion for underwater vehicles. It is commonly acknowledged that magnetic fields higher than 10 Teslas are, although achievable, not practical in large scale engineering applications. Therefore, for smaller vehicles, the possible applications of sea water MHD propulsion are in low speed ROV's and UAV's, with lower magnetic fields. The electric sources can be from batteries, fuel cells, or generators driven by the long endurance version of the stored chemical energy propulsion system (SCEPS) concept.[17] The high magnetic fields required by the torpedo applications appear to

be long-term goals to be accomplished.

On a more encouraging note, a 5-Tesla magnetic field appears to be adequately suited for propelling a class 2 submarine with reasonable speed and efficiency, as shown in Figs. 9 and 10. The electric power will most likely be nuclear driven. A class 2 submarine going with a speed of 36 knots would need 66 Mw of electric power for its MHD channels. Assuming the Rankine cycle efficiency of the nuclear propulsion plant is 33%, the required reactor thermal power would be at least 200 Mw. This, of course, does not include any other service power needed for the vehicle. Nevertheless, it, if not the same, is compatible in power capacity to the current nuclear submarine technologies.[18] In addition, a hybrid submarine having both the propeller screws and MHD channels may offer some strategic merits in underwater warfare.

Superconducting magnets are the essential elements of the sea water MHD propulsion technology, because they offer high fields at little electric consumption. They do need some cryogenic power to maintain low temperature. The liquid helium cooled superconducting magnets are somewhat hard to maintain due to helium leakage. The high-T_c superconducting materials offer the hope of more economical magnets, with much more cryogenic simplicity. Other important issues associated with sea water MHD propulsion are mainly in the electric conduction characteristics of the sea water. These are to be addressed in part in our future experimental studies.

An experimental facility is currently being constructed to study the current conducting characteristics of sea water. It is a closed flow loop that circulates the salt water through a test section. The salinity of the salt water will be properly controlled to simulate that of sea water. The test section is a rectangular channel made of plexiglass, with two parallel electrodes mounted on opposing walls. The electrodes are made of copper and plated with a 50 μ-inch platinum layer. The platinum is plated to prevent the electrolytic dissociation of the electrode material, and to provide a good gas evolution which results in good current conduction.

As the current is being supplied to the electrodes, hydrogen and chlorine micro bubbles will be formed at the cathode and anode, respectively. Perhaps the most important issue to be

addressed is how effective the current can be driven through the "flowing" salt water without saturating the electrolytic gas formation process. Since the performance of a thruster increases linearly with the sea water conductivity, enhancements of the fluid conductivity by seeding of strong electrolytes become worthwhile.

The electrolytic micro-bubbles on the electrodes can have significant impact on the turbulent fluid structure of the MHD flow in the channel. Its influence on the drag of an internal channel flow also affect the performance of the thruster. These are the issues remained to be addressed in our future experiments.

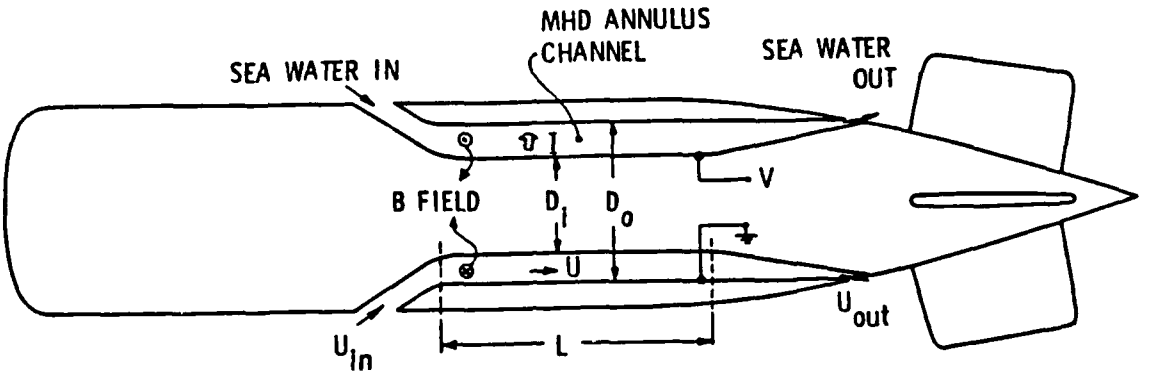

Figure 1(a) Submersible with an Annular MHD Channel

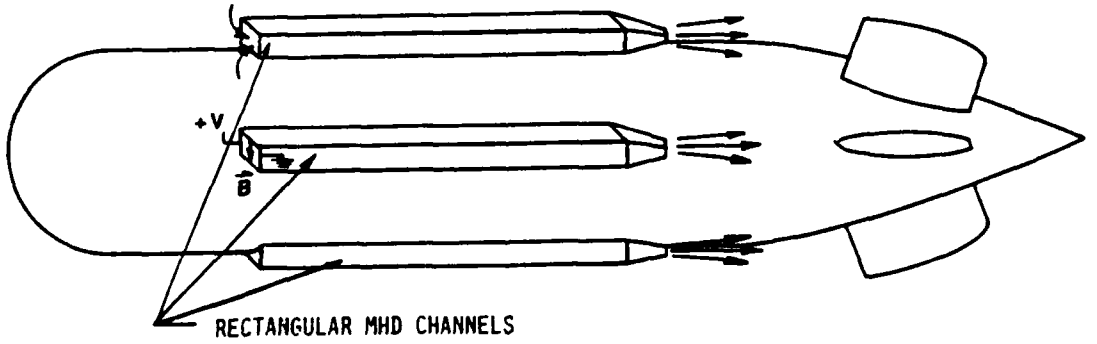

Figure 1(b) Submersible with Rectangular MHD Channels

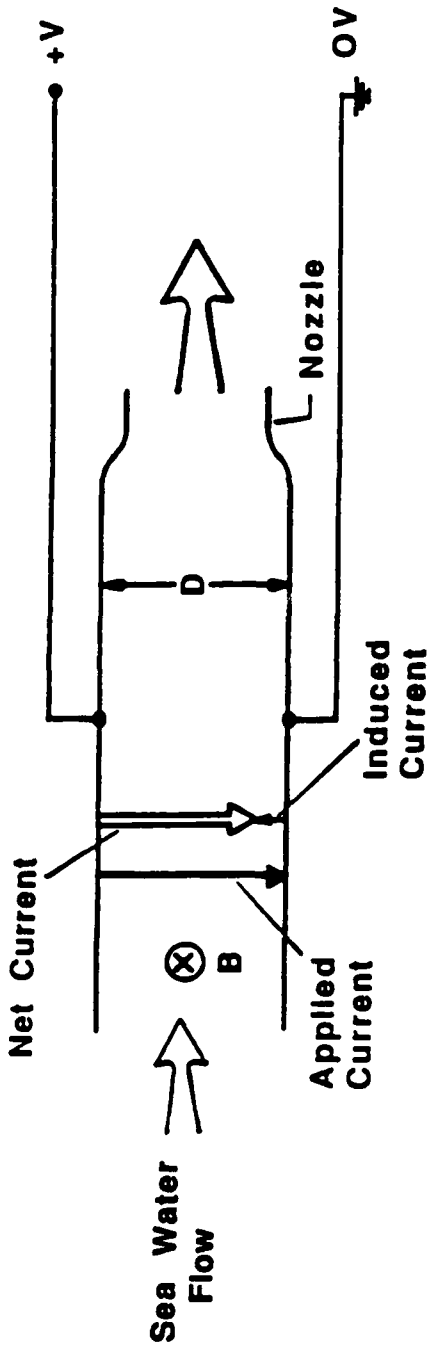

Figure 2 Schematic of a duct-type MHD Channel

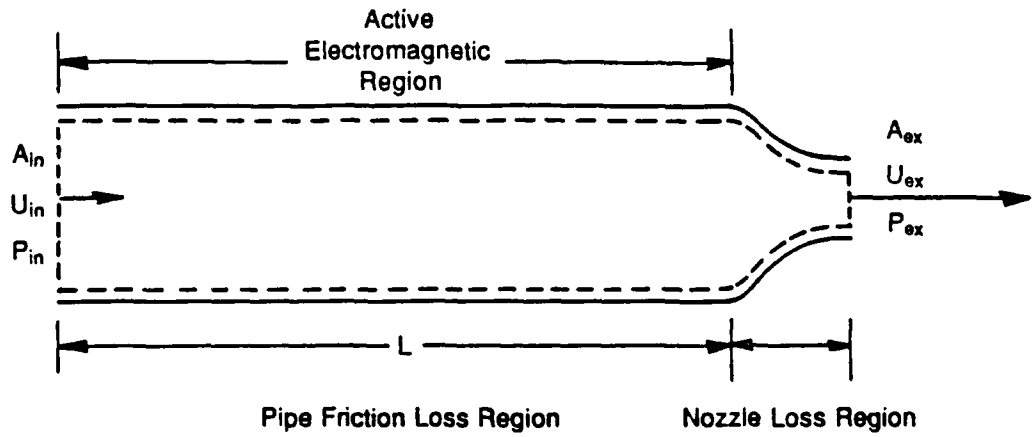

Figure 3 Control Volume #1

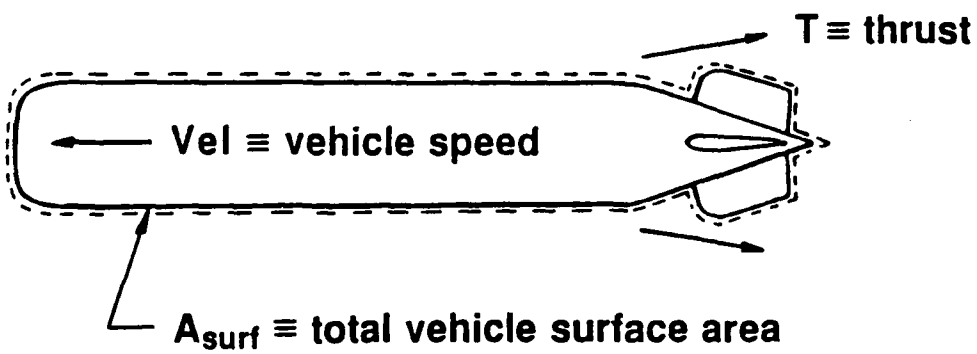

Figure 4 Control Volume #2

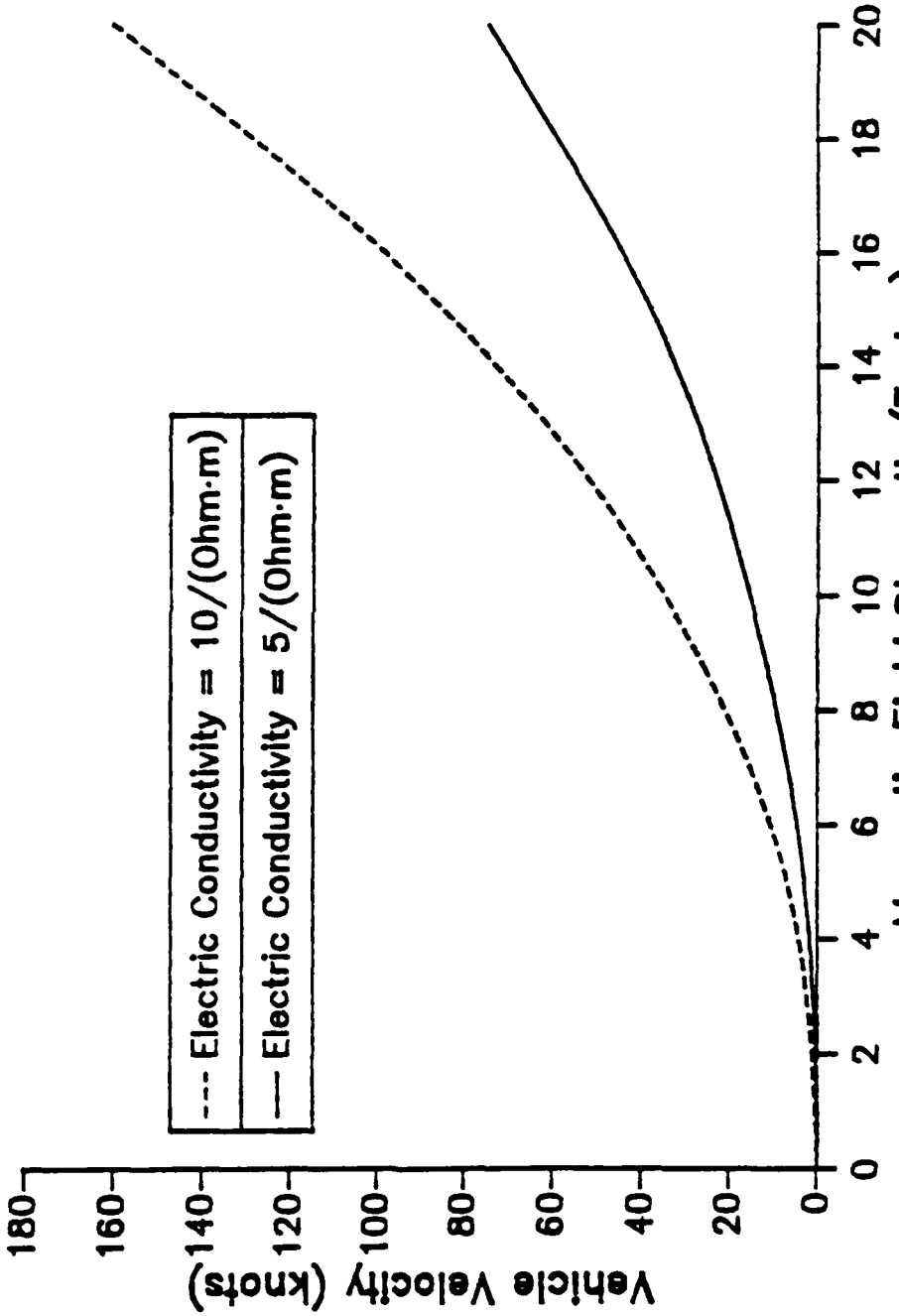

Figure 5 Velocity vs. Magnetic Field for Class 1 Vehicles.

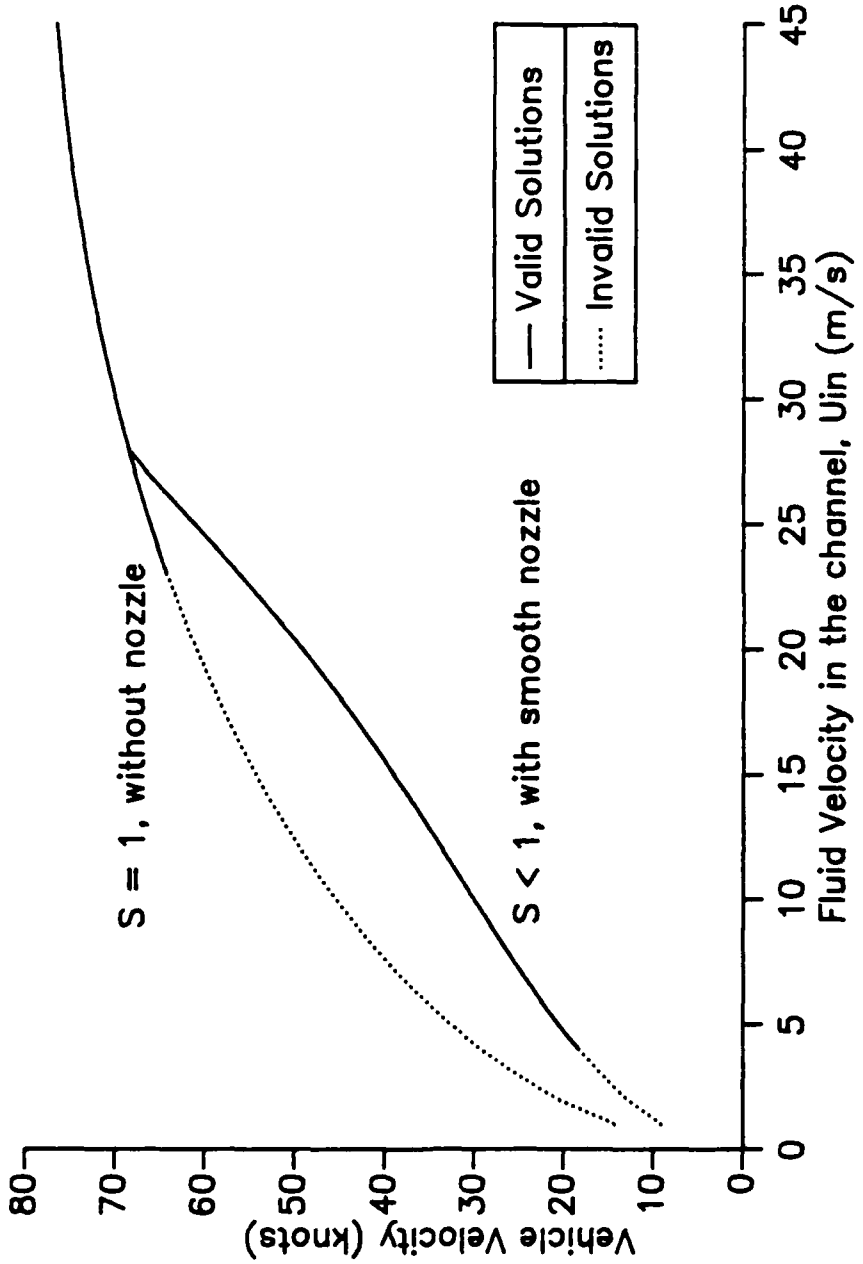

Figure 6 Velocity of Class 1 Vehicles at B = 20T.

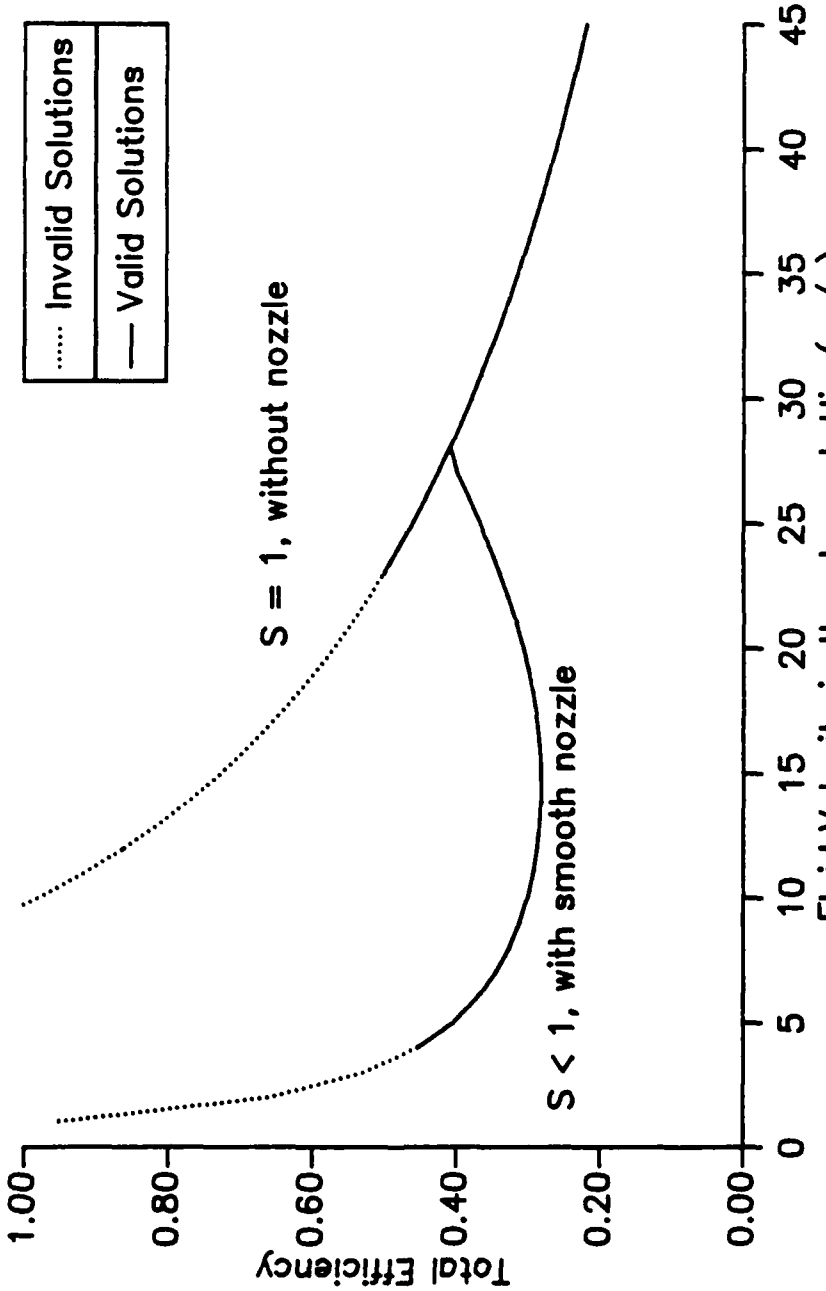

Figure 7 Total Efficiency of Class 1 Vehicles at B = 20T.

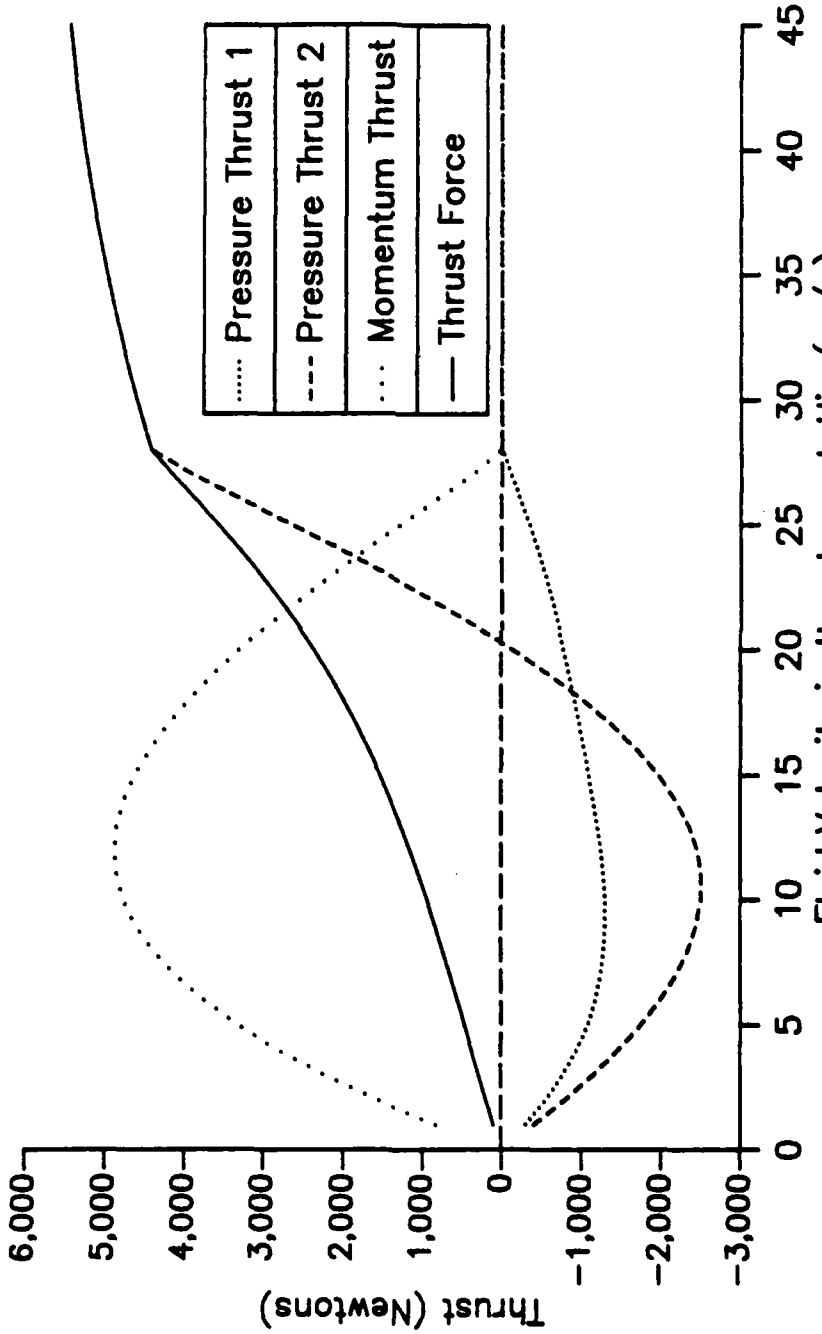

Figure 8 Thrust of Class 1 Vehicles at B = 20T.

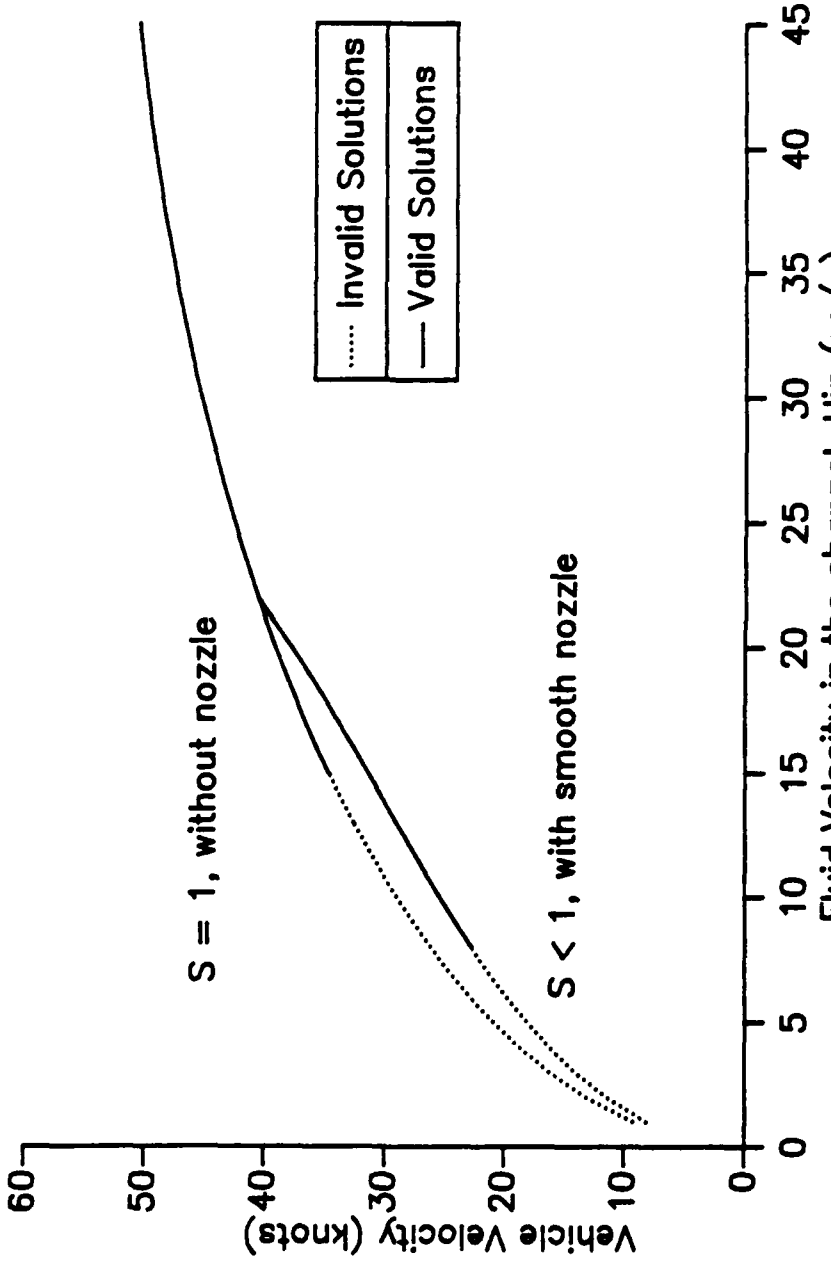

Figure 9 Velocity of Class 2 Vehicles at B = 5T.

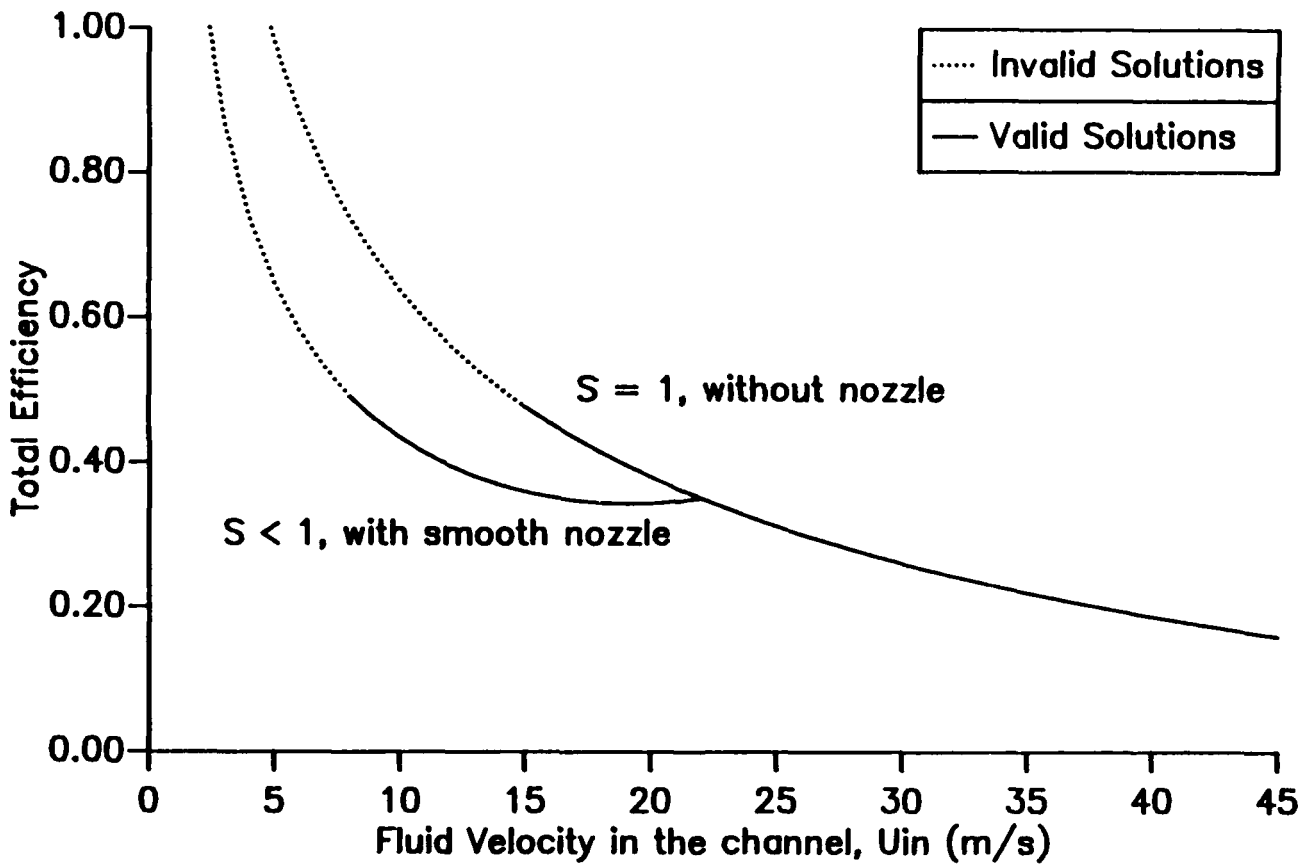

Figure 10 Total Efficiency of Class 2 Vehicles at B = 5T.

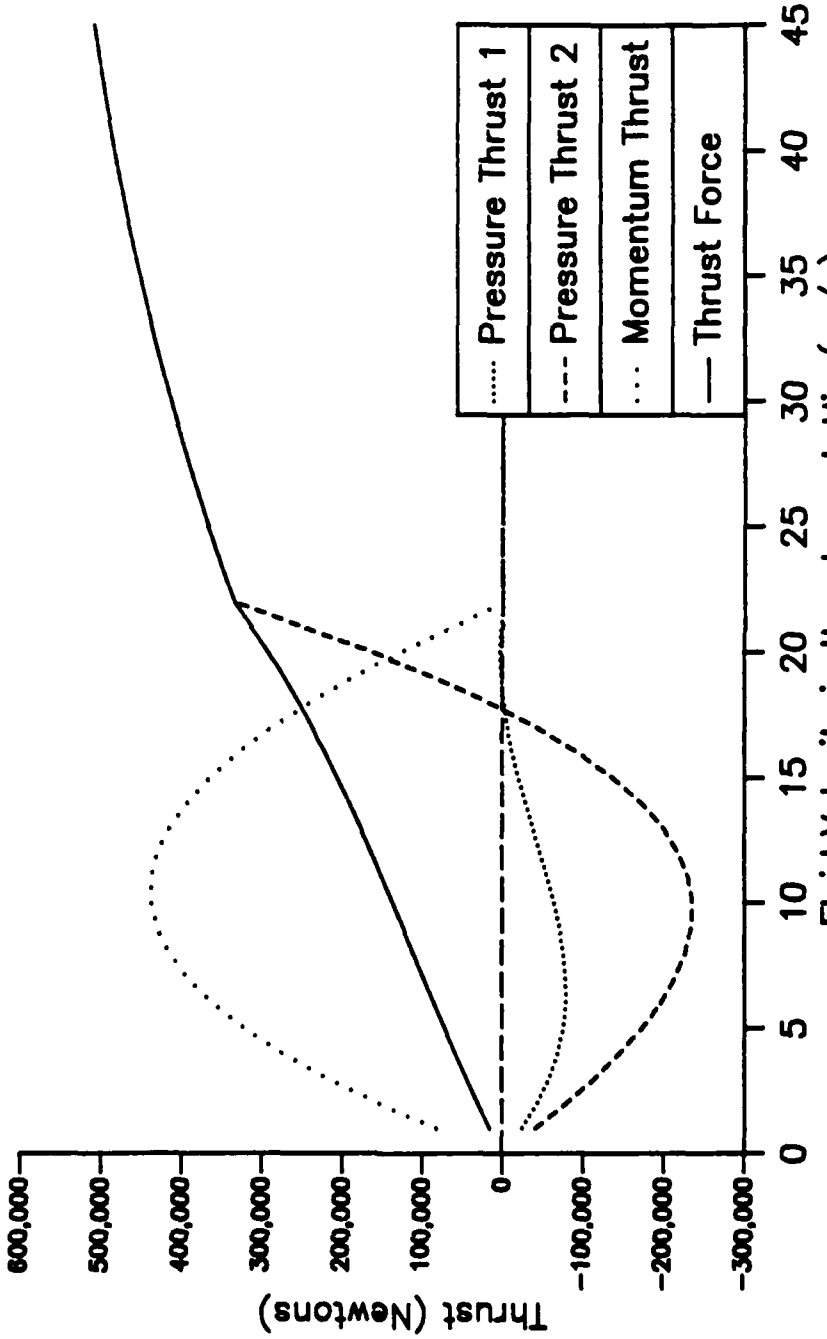

Figure 11 Thrust of Class 2 Vehicles at B = 5T.

PART II
SEA WATER CONDUCTIVITY ENHANCEMENT

II.1 Introduction

Marine vehicle propulsion using magnetohydrodynamic (MHD) thrusters by applying the JxB Lorentz force on the sea water around the vehicle has been a technical speculation for some time.[1-7] It offers the advantages of having minimal mechanical moving parts, having no need for propellers, and therefore giving off little acoustic noise which is specially important in naval applications. The velocity and efficiency performances of marine vehicles using such a propulsion technology depend linearly on the electrical conductivity (σ) of the medium, and on the square of the magnetic field strength (B).[19] Previous studies have suggested that multi-Tesla magnets are very essential to achieve any kind of success in this technology. While it seems more logical to increase the magnetic field than to increase the medium conductivity, there are technical limitations and economical considerations that prohibit the increase of magnetic field in an already multi-Tesla regime. It then leaves the only option of trying to enhance the conductivity of sea water.

There are numerous ways of locally increasing the conductivity of sea water. Into a flowing sea water channel, one can apply seedings of metal particles or powders to increase the average mixture conductivity. Or one can irradiate the flow with Lasers or ionizing radiations to increase the ionic concentration, and therefore increase the sea water conductivity. None of them seems to have been practical.[20] The only method that appears to hold some promise is to seed strong electrolytes into the sea water flow through injection and turbulence mixing, and as a consequence, to increase the concentration of H^+ or OH^-.

Sea water has an average specific conductance of about 4 to 5 $\frac{1}{\Omega m}$. This part of the report attempted to verify this value from the electro-chemical points of view. As the major salt constituents of sea water are generally known, mole concentrations of individual salts can be deduced. Since $NaCl$ turned out to be the dominant electrolytic salt (0.5 mol/liter) among

others such as $MgCl_2$ (0.042 mol/liter) and $MgSO_4$ (0.015 mol/liter), the conductivity of sea water can be calculated from the molar ionic conductances of individual ionic elements at their appropriate concentrations. For the simple synthetic sea water selected, the computed conductivity turned out to be very close to the above suggested value.

It is desirable to, as suggested earlier, increase the conductivity of the sea water that flows in the MHD thruster to improve the propulsion performances. Seeding strong electrolytes, acids or bases, in sea water stream is generally accepted as the most effective method to enhance the conductivity. This work investigated the effectiveness of three different compounds, namely HCl, H_2SO_4 and $NaOH$. The reason for choosing these strong acids and base is because of the high ionic conductances and mobilities of H^+ and OH^- ions. Other important properties such as the degree of electrolyte dissociation, and the solubility in phase equilibrium condition are also considered.

II.2 Analyses

The fact that aqueous solutions of certain materials call "electrolytes" conduct an electric current provides the most direct evidence for the idea that ions capable of independent motion are present. Measurements of the conductivity of aqueous solutions are made with a conductivity cell using an alternating current to prevent build-up of charges of opposite sign near the two electrodes There will be little electric resistance at the metal/solution interface, and the conduction of electricity obeys the Ohm's law. That is, the current flowing through the cell is proportional to the voltage across the cell. It is therefore possible to assign a resistance, R, similar to that of a metallic conductor, to the cell.

More conveniently the conductance of an electrolyte solution is defined as the reverse of the resistance,

$$L = \frac{1}{R}. \tag{22}$$

Similar to metallic conductor, the solution resistance depends on the cross-sectional area A and

the length l of the region between the electrodes. It is written as,

$$R = \rho \frac{l}{A}, \tag{23}$$

where ρ is the specific resistance and is the proportionality factor that corresponds to the resistance of a cell of unit cross-sectional area and unit length. One can also write,

$$L = \sigma \frac{A}{l}, \tag{24}$$

where σ, the specific conductance, can be thought of as the conductance of a cube of the electrolyte solution of unit dimensions. The specific conductance is normally obtained from the measured value of R, which gives $L = 1/R$, and l and A of the cell. In practice, it is more convenient to deduce l and A, or rather the "cell constant" l/A, from a measurement of L when the cell is filled with a solution of known specific conductance. Once the cell constant is determined, the same cell can be used to deduce the σ for an unknown solution from the measurement of L, Eq. (24). The cell constant is almost always determined by using a solution of KCl.

Solutions of different concentrations have quite different specific conductances, simply because a given volume of solution contains different amounts of electrolytes. It is then helpful to define another measure of conductance, known as "molar conductance" Λ.[21] Supposed a conductivity cell in which the electrodes are 1 meter apart and of sufficient area that the cell holds the amount of solution which contains 1 mole of solute, then the conductance of such a cell is the molar conductance. Considering a solution of concentration c, i.e. c moles of solute in a liter, its molar conductance will be,

$$\Lambda = 10^{-3} \frac{\sigma}{c} (\Omega^{-1} m^2 mol^{-1}). \tag{25}$$

Many precise measurements of molar conductance were made by F. Kohlrausch and his coworkers between 1860 and 1880. The values of molar conductance tabulated for different electrolytes at different concentrations are useful in many ways. Among them is the determination

of the specific conductance of sea water. Before the determination of sea water conductivity, it is necessary to define the limiting molar conductance, Λ°. It is the molar conductance at the condition of infinite dilution. At this condition, according to Kohlrausch, the conductance of an electrolyte is treated as being made up of contributions from the individual ions. Let ν_+ be the number of positive ions and ν_- be the number of negative ions by the formula of the electrolyte. Then, if λ_+° and λ_-° are the molar ionic conductances of the positive and negative ions respectively, we have the relation,

$$\Lambda^\circ = \nu_+\lambda_+^\circ + \nu_-\lambda_-^\circ. \tag{26}$$

The values of λ_+° and λ_-° for various ions are also available for most electrolytes.[22] Here the conductivity of sea water, or a closely simulated instant ocean, can be estimated based on a firm theoretical ground.

In a synthetic sea water, the three major salts are $NaCl$, $MgCl_2$ and $MgSO_4$, with $NaCl$ being the dominant one ($c \approx 0.5015 mol/l$). The concentrations for $MgCl_2$ and $MgSO_4$ are 0.0419 and 0.0152, respectively, and can be treated as infinitely diluted. The contributions from the other salts are neglected without making significant difference in conductivity estimation. The molar conductance of $NaCl$ at the stated concentration is $\Lambda \approx 0.0085 \Omega^{-1} m^2 mol^{-1}$, and it contributes to a specific conductance of,

$$\sigma(NaCl) = 0.0085 \times 0.5015 \times 10^3 = 4.26 \Omega^{-1} m^{-1},$$

The limiting molar conductances of the other two salts are, from Eq.(26),

$$\Lambda(MgCl_2) = 1 \times 0.0106 + 2 \times 0.00763 = 0.0259 \Omega^{-1} m^2 mol^{-1},$$

and,

$$\Lambda(MgSO_4) = 1 \times 0.0106 + 1 \times 0.0160 = 0.0266 \Omega^{-1} m^2 mol^{-1}.$$

Their contributions in sea water's specific conductance are,

$$\sigma(MgCl_2) = 0.0259 \times 0.0419 \times 10^3 = 1.08 \Omega^{-1} m^{-1},$$

and,

$$\sigma(MgSO_4) = 0.0266 \times 0.0152 \times 10^3 = 0.40\Omega^{-1}m^{-1}.$$

Thus, the estimated specific conductance of the synthetic sea water is,

$$\sigma_{sw} = 4.26 + 1.08 + 0.40 = 5.74\Omega^{-1}m^{-1}.$$

This calculated value of conductivity of a synthetic sea water is rather close to the measured ocean water conductivity, which varies from 4 to 5 $\Omega^{-1}m^{-1}$ depending on the location and temperature. The slight over estimation is due to the assumption of infinite dilution for some of the salts.

Next we shall consider the effect of electrolyte seeding in sea water conductivity enhancement. An average sea water conductivity is assumed to be 5 $\Omega^{-1}m^{-1}$. The three electrolytes to be compared are HCl, H_2SO_4 and $NaOH$. The basis for the choice of these electrolytes is due to the fact that they strong electrolytes and have high molar ionic conductances and high ionic mobilities. In the practice of conductivity enhancement by electrolyte injection, it is important to define the volumetric mixing ratio r. That is the ratio of the volume of injected fluid to that of the mixed sea water. In a sea water MHD thruster the main sea water flow in the channel is very large and it is impractical to have a volumetric mixing ratio higher than a few percent. Therefore, under thorough mixing, the final conductivity of the sea-water/electrolyte solution will be the conductivity of the original sea water plus the contribution from the seeding as if it is mixed with fresh water. The final conductivity will be,

$$\sigma = \sigma_{sw} + \sigma_a. \tag{27}$$

Since the volumetric mixing ratio is much less than 1, σ_{sw} remains to be 5 $\Omega^{-1}m^{-1}$. σ_a is the contribution of the electrolyte to the final conductivity. Its value is related to the mole concentration of this seeding electrolyte at the final mixed state, which in turn is related to the original electrolyte concentration and the volumetric mixing ratio. Here we shall adopt a linear additive rule of solution volume. It simply means that the volume of the solution is exactly

the sum of the volumes of the solute and solvent, and there is no net change of volume after mixing. All the three seeding candidates in their injectable form (i.e. liquid) cannot be 100% pure due to solubility limitation. The common aqueous solutions of them with different weight percentages, mole concentrations and densities are tabulated in Table 1.[23] Then, the final mole concentration of the electrolyte after thorough mixing is,

$$c = rc_o. \tag{28}$$

As the molar conductances of the three electrolytes are readily tabulated against mole concentration (discussed next), the values of σ_a can be obtained through Eq. (25). Finally, the conductivity enhancement to sea water can be estimated, Eq. (27).

II.3 Results

The molar conductances of HCl, H_2SO_4 and $NaOH$ as functions of mole concentration are available from ref. 21. As shown in Table 2, the comparison is based on different mole concentrations of electrolytes per liter of sea water solution at room temperature. In addition to the tabulated values of molar conductance, the specific conductance of the original sea water, that of the added electrolyte, as well as the final specific conductance are all listed. Contradicting to the common perception that HCl is the choice of electrolyte due to its small molecular size, H_2SO_4 appeared to be more effective in enhancing the sea water conductivity on the same mole concentration basis. The main reason is that each H_2SO_4 molecule, when dissociates, gives off two H^+ ions, twice of that of HCl.

In Figure 12, the effect of volumetric mixing ratio to sea water conductivity is shown. The aqueous solutions of electrolytes are the ones listed in Table 1. At a volumetric mixing ratio, the final mole concentrations of electrolytes were first determined by Eq. (28). The final specific conductances of the solutions are then obtained by interpolation with Table 2. Again, it has shown that H_2SO_4 is more effective than the other two in enhancing the conductivity of sea water. It is noted that it takes the least amount of H_2SO_4 volume ($r \approx 0.006$) to double the

conductivity of sea water. The volumetric mixing ratios needed by HCl and $NaOH$ to achieve the same are 0.011 and 0.018, respectively.

II.4 Discussion

In the practical mixing procedures, only H_2SO_4 can be obtained in an extremely concentrated form (96% wt), making it easy to mix small volume of H_2SO_4 to the sea water. Common concentrated HCl is about 37% wt, since HCl in its pure form is at the gaseous state. Although aqueous $NaOH$ solution can be concentrated up to 50% wt, common $NaOH$ solution is about 10% wt, making it also unattractive for mixing. As mixing is likely to be accomplished by constant displacement pump injection, H_2SO_4 stands out better for both its high conductivity and high concentration. The advantage of using concentrated H_2SO_4 as seeding electrolyte in sea water is because of its abundance of H^+ ions. Not only H^+ has higher molar ionic conductance than that of OH^- (0.035 vs 0.020 $\Omega^{-1}m^2mol^{-1}$), but also it has higher ionic mobility than that of OH^-. Ionic mobility is a measure of ion's velocity under a unit electric field in the solution. The ionic mobilities for H^+ and OH^- are 36.3×10^{-8} and 20.5×10^{-8} $m^2s^{-1}V^{-1}$, respectively. Since H^+ cations move much faster than the negative anions in an acid solution, the electric current is mainly carried out by the H^+ ions. Thus, the desirable condition to increase conductivity is to have as much H^+ ions in the solution as possible. Between the 96% wt H_2SO_4 and 37% wt HCl aqueous solutions, H_2SO_4 does have the slight disadvantage of being more viscous. Therefore, it requires more power from the injection pump.

While the electric current is flowing across the electrodes, electrolytic micro-bubbles tend to accumulate at both electrodes. That can increase the overall resistance of the sea water mixture. The presence of gas bubbles is especially noticeable at the cathode since H_2 gas is highly non-condensable. Nevertheless, in MHD thrusters, the sea water flow between the electrodes in the channel is so high as to be able to flush away the bubbles. As a consequence, the resistance may not increase significantly. This, however, is pure speculation and experimental verification is recommended.

Table 1 Properties of common seeding electrolytes at 20°C

	wt% (%)	Formula Weight	Density (gm/ml)	c_o (mol/l)
HCl	37	36.47	1.19	12.1
H_2SO_4	96	98.08	1.84	18.0
$NaOH$[1]	50	40.00	1.52	19.0

1) This $NaOH$ solution is in the form of highest concentration. A common $NaOH$ aqueous solution is about 10% wt.

Table 2 Conductivity contributions of different electrolytes

c		HCl			H_2SO_4			$NaOH$	
	Λ	σ_a	$\sigma_{sw}+\sigma_a$	Λ	σ_a	$\sigma_{sw}+\sigma_a$	Λ	σ_a	$\sigma_{sw}+\sigma_a$
(mol/l)	$\Omega^{-1}m^2mol^{-1}$	$\Omega^{-1}m^{-1}$	$\Omega^{-1}m^{-1}$	$\Omega^{-1}m^2mol^{-1}$	$\Omega^{-1}m^{-1}$	$\Omega^{-1}m^{-1}$	$\Omega^{-1}m^2mol^{-1}$	$\Omega^{-1}m^{-1}$	$\Omega^{-1}m^{-1}$
0.0	0.042616	0.0	5.0	0.08592	0.0	5.0	0.02465	0.0	5.0
0.0005	0.042274	0.021137	5.021137	0.08262	0.04131	5.04131	0.02440	0.01220	5.01220
0.001	0.042136	0.042136	5.042136	0.07990	0.07990	5.07990	0.02430	0.02430	5.02430
0.01	0.04120	0.4120	5.4120	0.06728	0.6728	5.6728	0.02354	0.2354	5.2354
0.1	0.039132	3.9132	8.9132	0.05016	5.016	10.016	0.02116	2.116	7.116
1.0	0.03328	33.28	38.28	0.03000	30.00	35.00	0.01362	13.62	18.62

1) Λ: molar conductance.

2) σ_{sw}: average sea water conductivity.

3) σ_a: conductivity of the added electrolyte.

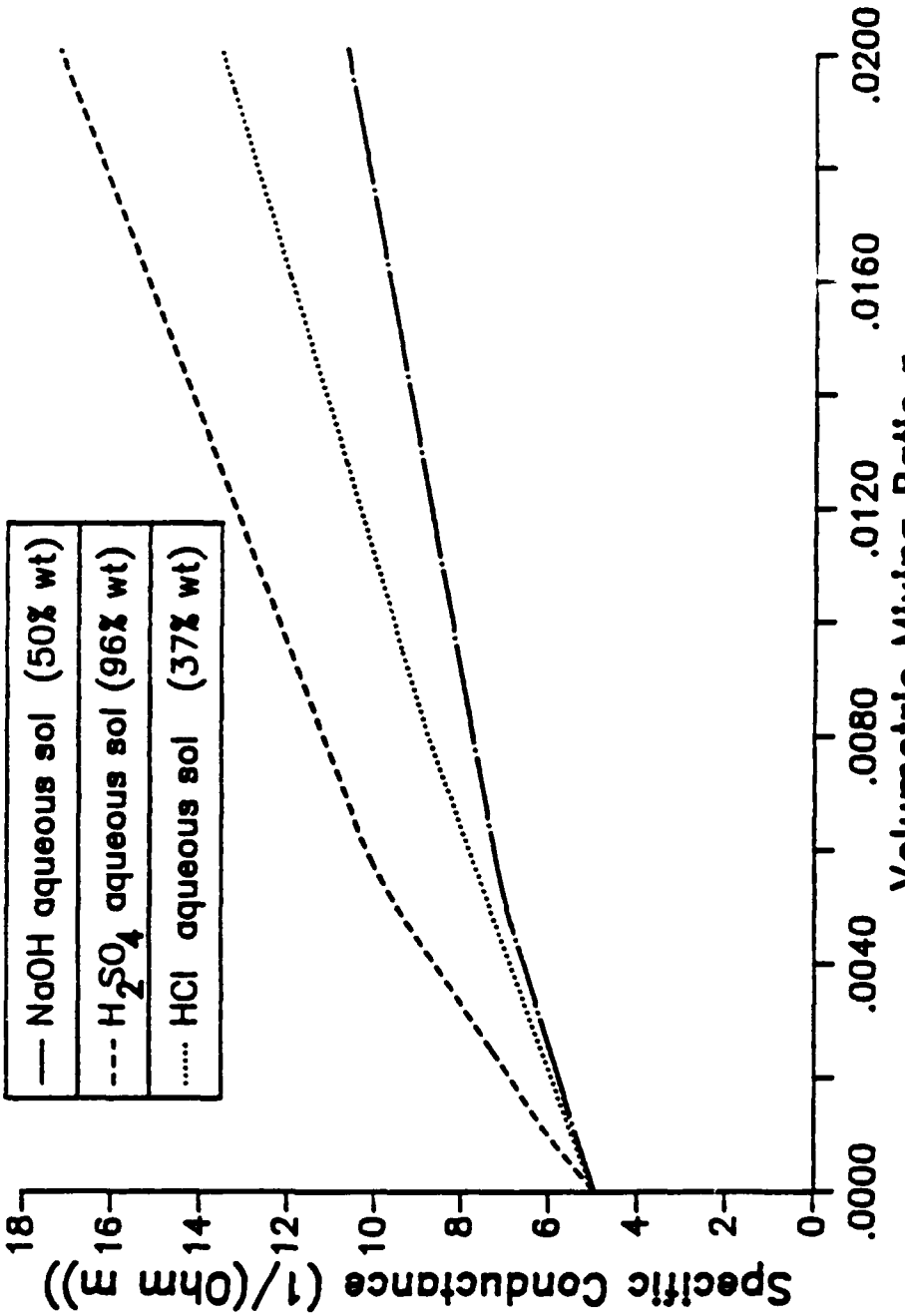

Figure 12 Conductances of sea water seeded with electrolytes.

PART III
STATUS OF CURRENT SUPERCONDUCTIVITY WORKS

Survey of the current literature clearly demonstrates that after very extensive research for close to three years, bulk high-T_c superconductors show rather low capability for current carrying, when compared to thin film conductors. The physics community has ascribed these differences to the existence of weak-links in bulk materials. The term weak-links should be viewed as a concept, which incorporates a number of materials, as well as, fundamental solid state behaviors. Oxygen stoichiometry, phase pur y, grain orientation, short correlation length (λ), large penetration depth (ξ), and the compositions and structures of interparticle interfaces, have been identified as critical factors contributing to the phenomenon dubbed as weak-links. Researchers are therefore careful to separate the intrinsic behavior of single superconducting grain from the interconnecting path at grain boundaries.

In simple terms, it is now acceptable that the critical current through a superconducting single crystal is affected by oxygen stoichiometry, crystal structure and the orientation of the Cu-O chains with respect to the field vector (**B**). The interconnecting grain boundaries have been treated as non-conducting, or semi-conducting Josephson-like junctions.

The challenge to the effective consolidation of a bulk superconductor is dictated by the need to balance structure, orientation, chemistry, and flux pinning environment within the limits of reproducibly adjustable parameters such as temperature, heating and cooling rates, oxygen environment, starting powder purity and magnetic fields, which may be available during consolidation.

Research established a rather narrow, optimal temperature for consolidation of powder by the sintering process. Sintering at 920-930°C maintains the phase equilibrium while promoting natural grain growth along the Cu-O chain directions.

Annealing has been established as a second control parameter leading to further optimization of the consolidation process. After annealing at 400°C for a few hours, two distinct

superconducting phases evolve, i.e., the phase showing a T_c at 90K and a phase showing T_c at about 60K. The volume fraction of the 60K phase continuously decrease with increasing annealing time, with no detectable change in oxygen concentration. These findings support the physicists' assertion that hole concentration and oxygen ordering play a major role in the intrinsic superconducting behavior of Y-Ba-Cu-O materials.

Researchers in the United Kingdom are developing a growth method known as flux growth. This method yields highly textured and chemically uniform samples. Data show that texturing is confined to only a few thousand angstroms of the surface of the grain, yielding, for the layers, current densities of the order of a few thousand A/cm^2. One cannot but make a comparison of these data with thin films, which are highly oriented, homogeneous, and rather limited to thickness of fractions of microns. Highest current densities, reported by a rather large number of investigators, were all obtained with thin films.

Melt processing, texturing and the utilization of Ag or Ag-O additions are being explored by industrial researchers in an attempt to produce filamentary conductors. Ag and Ag-O are introduced as a means to overcome the contributions of grain boundaries to the weak-link phenomenon, while melt processing and texturing are employed to optimize the intrinsic behavior of superconducting grains.

In these studies, wires are produced by the powder-in-tube technique. Monofilamentary wires are produced by filling pre-reacted high temperature superconducting powder into an Ag tube, and working of the composite by rolling, swagging and wire drawing. Multifilamentary wires can be produced by bundling monofilamentary wires in an outer Ag tube and subsequent cold working.

Ag has been chosen because it does not react with the superconductor and does not degrade the superconducting properties. Furthermore, Ag is transparent to oxygen at elevated temperature so that the required oxygen content can be achieved through heat treatment of the wire in oxygen or air.

After cold working, the high temperature superconducting composite wires are annealed at high temperature. Due to the melting point of Ag at 960°C, the heat treatment temperature is limited to values below this temperature. The oxygen content is adjusted close to O_7 by additional heat treatments, i.e., at 560°C, or by slow cooling through this temperature regime.

Critical currents of the order of a few thousand A/cm^2 at zero field, were obtained in Y-Ba-Cu-O-Ag composites by flattening the wire to a thin tape. This improvement is not intrinsic, but rather reflects the fact that critical current is limited by the self field of the flowing current, which in turn is proportional to the diameter of the conductor.

The rather strong effects of external field raise a few disturbing questions. The concept of flux pinning is not yet well understood for high temperature superconductors. Applications of the Ginsburg-Landau phenomenological theory yield correlation length, λ, of the order of only a few angstroms, while indicating rather large field penetration depth, ξ, of the order of a few thousand angstroms. The debates over the applicability of the phenomenological concepts, and the implications of their findings, if they are applicable, are far from being concluded. One should note, however, that the general findings related to the behavior of thin films, the rather high sensitivity to orientation, and the strong effects of external fields on T_c, are not inconsistent with the results of the Ginsburg-Landau generalized approach.

Rather high current densities have been reported by investigators employing a melt growth and quench technique. In this process, the material is heated to temperatures above 1200°C, in the Y_2O_3 plus liquid regime. After quenching to room temperature, the sample is heated to about 1200°C and slowly cooled through a thermal gradient in oxygen atmospehre. These procedures yield materials with high degrees of homogeneity and preferred orientation. It is also argued that this method reduces significantly resistivities across grain boundaries by eliminating mono-layered contaiminations intrinsic to sintered powder products. Currnts of the order of $10^4 A/cm^2$ were obtained in field of the order of 1T, increasing to $10^5 A/cm^2$ in zero field.

In a further modification of the melt-quench processing, samples are heated fast to 1100°C and cooled down rapidly after about ten minutes hold at 1030°. A very slow cooling rate from

1030° to 980°C, where a peritectic reaction takes place has been shown to be essential for high critical currents. DC measurements at $B = 0$ at 77K showed critical currents of the order of $1.8 \times 10^4 A/cm^2$ with a 1 μs pulse.

The work on bismuth (Bi) compounds is at rather early stages. Data show, however, that these compounds have the potential of superceding the YBaCuO compounds in their current carrying capacity. Filamentary conductors, produced by melt-quench-drawing process, show potential for performance superceding the $NbTi$ and Nb_3Sn metallic superconductors. Data shown in Figure 13, obtained from reported work at Vacuumschelze in Germany, illustrates this point.

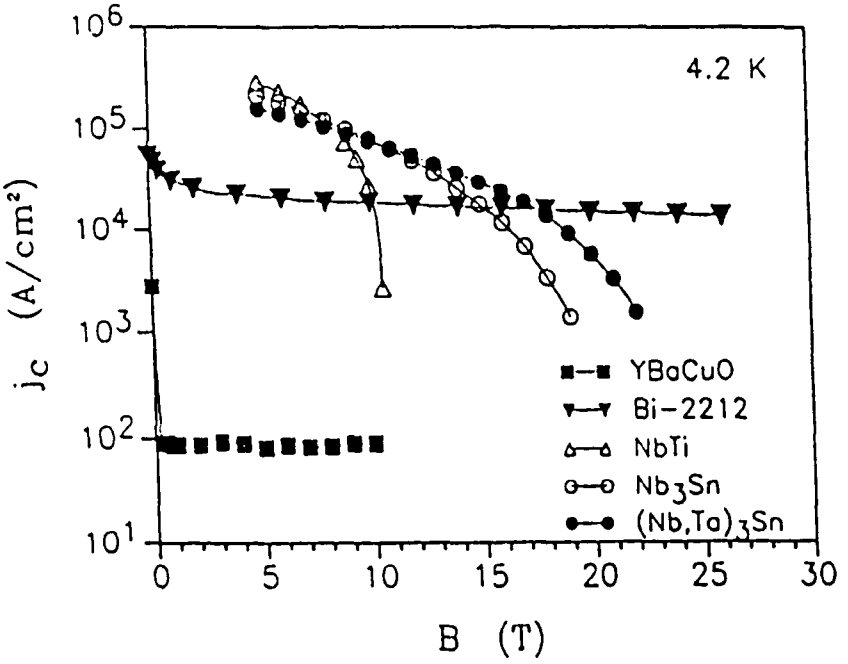

Figure 13
Critical current density of Bi-2212/Ag and $YBa_2Cu_3O_7$/Ag-wire at 4.2K in comparison with commercial NbTi, Nb_3Sn, and $(Nb,Ta)_3$ multifilamentary wires (non-copper J_c) as produced by Vacuumschmelze.

REFERENCES

[1] W. A. Rice, U. S. patent 2997013, August 12, 1961.

[2] J. B. Friauf, "Electromagnetic Ship Propulsion," *J. of Amer. Soc. of Naval Engrs.*, Feb., 1961, pp 139-142.

[3] O. M. Phillips, "The Prospects for Magnetohydrodynamic Ship Propulsion," *J. of Ship Research*, March, 1962, pp 43-51.

[4] R. A. Doragh, "Magnetohydrodynamic Ship Propulsion using Superconducting Magnets," Soc. of Naval Architects and Marine Engineers, Annual Meeting, New York, Nov. 14, 15, 1963.

[5] S. Way, "Propulsion of Submarines by Lorentz Forces in the Surrounding Sea," Amer. Soc. of Mechanical Engrs, Paper 64 WA/ENER7, Nov., 1964.

[6] S. Way and C. Devlin, "Prospects for the Electromagnetic Submarine," Collection of Technical Papers, AIAA 3rd Propulsion Joint Specialist Conference, Washington D. C., July 17-21, 1967, Paper # 67-432.

[7] A. P. Baranov, "Future of Magnetohydrodynamic Ship Propulsion," *Sudostroyeniye*, No. 12, 1966, pp 3-6.

[8] A. Iwata, Y. Saji and S. Sato, "Construction of Model Ship ST-500 with Superconducting Electromagnetic Thrust System," Proc. ICEC 8, 1980, pp 775-784.

[9] E. Tada, Y. Saji, K. Kuroshi and T. Fujinaga, "Fundamental Design of a Superconducting EMT Icebreaker," *Trans. IMarE(C)*, Vol. 97, Conf. 3, Paper 6, pp 49-57, 1984.

[10] Y. Sasakawa, K. Imaichi, E. Tada and S. Takezawa, "Japanese Experimental Ship with the Superconducting Electromagnetic Thruster," Paper presented in the Applied Superconducting Conference in Osaka University, Japan, Oct. 17, 1988.

[11] G. T. Hummert, "An Evaluation of Direct Current Electromagnetic Propulsion in Sea Water," Office of Naval Research Project Report, 79-9B2-EMSUB-R1, 1979.

[12] J. P. Waggener, "Friction Factor for Pressure Drop Calculation," *Nucleonics*, vol. 19, no. 11, 1961, pp 145-147.

[13] G. L. Tuve and L. C. Domholdt, **Engineering Experimentation**, McGraw Hill, 1966, pp 369-381.

[14] G. P. Sutton, **Rocket Propulsion Elements**, John Wiley & sons, 1976, pp 13-23.

[15] T. C. Gillmer and B. Johnson, **Introduction to Naval Architecture**, United States Naval Institute, Annapolis, 1982, p 220.

[16] Sv. Aa. Harvald, **Resistance and Propulsion of Ships**, John Wiley and Sons, 1983, pp 98-100.

[17] T. G. Hughes, R. B. Smith and D. H. Kiely, "Stored Chemical Energy Propulsion System for Underwater Applications," *Journal of Energy*, AIAA, Vol. 7, No. 2, 1983, pp 128-133.

[18] T. Stefanick, "The Non-acoustic Detection of Submarines," *Scientific American*, vol. 258, no. 3, March, 1988, pp. 41-47.

[19] T. F. Lin and J. B. Gilbert, "Sea Water Magnetohydrodynamic Propulsion for Underwater Vehicles," Proceedings Second ONR Propulsion Meeting in Energetic Material Combustion, Combustion Diagnostics and Underwater Propulsion, Irvine, Calif., Oct. 17-18, 1989.

[20] C. Young, "Conductivity Enhancement in Sea Water," Proceeding ONR/DARPA Workshop in Magnetohydrodynamic Submarine Propulsion, San Diego, Calif., Nov. 16-17, 1989.

[21] G. M. Barrow, **Physical Chemistry**, McGraw Hill, 5th ed., 1988, pp 306-309.

[22] D. A. MacInnes, **The Principles of Electrochemistry**, Reinhold Publishing Co., 1939.

[23] R. H. Perry and C. H. Chilton, ed., **Chemical Engineering Handbook**, 5th ed., McGraw Hill, 1973.